ELSEVIER

Localized multi-scale energy and vorticity analysis II. Finite-amplitude instability theory and validation

X. San Liang [a,*], Allan R. Robinson [a,b]

[a] *Harvard University, School of Engineering and Applied Sciences, Cambridge, MA, USA*
[b] *Harvard University, Department of Earth and Planetary Sciences, Cambridge, MA, USA*

Abstract

A novel localized finite-amplitude hydrodynamic stability analysis is established in a unified treatment for the study of real oceanic and atmospheric processes, which are in general highly nonlinear, and intermittent in space and time. We first re-state the classical definition using the multi-scale energy and vorticity analysis (MS-EVA) developed in Liang and Robinson [Liang, X.S., Robinson, A.R., 2005. Localized multiscale energy and vorticity analysis. I. Fundamentals. Dyn. Atmos. Oceans 38, 195–230], and then manipulate certain global operators to achieve the temporal and spatial localization. The key of the spatial localization is *transfer-transport separation*, which is made precise with the concept of *perfect transfer*, while relaxation of marginalization leads to the localization of time. In doing so the information of transfer lost in the averages is retrieved and an easy-to-use instability metric is obtained. The resulting metric is field-like (Eulerian), conceptually generalizing the classical formalism, a bulk notion over the whole system. In this framework, an instability has a *structure*, which is of particular use for open flow processes. We check the structure of baroclinic instability with the benchmark Eady model solution, and the Iceland–Faeroe Frontal (IFF) intrusion, a highly localized and nonlinear process occurring frequently in the region between Iceland and Faeroe Islands. A clear isolated baroclinic instability is identified around the intrusion, which is further found to be characterized by the transition from a spatially growing mode to a temporally growing mode. We also check the consistency of the MS-EVA dynamics with the barotropic Kuo model. An observation is that a local perturbation burst does not necessarily imply an instability: the perturbation energy could be transported from other processes occurring elsewhere. We find that our analysis yields a Kuo theorem-consistent mean–eddy interaction, which is not seen in a conventional Reynolds stress framework. Using

* Corresponding author. Current address: Courant Institute of Mathematical Sciences, 251 Mercer Street, New York, NY 10012, USA.
  E-mail address: sanliang@courant.nyu.edu (X. San Liang).

the techniques of marginalization and localization, this work sets up an example for the generalization of certain geophysical fluid dynamics theories for more generic purposes.

1. Introduction

We apply the multi-scale energy and vorticity analysis (MS-EVA) developed in the first part of this paper (Liang and Robinson, 2005; LR1 hereafter) to formulate a localized instability analysis for processes of finite amplitude and with spatial and temporal intermittence. This formalism is then validated with three benchmark problems. In the sequel to this paper, Liang and Robinson (2004; LR2 hereafter), it will be applied to the study of a real ocean problem.

Stability is an important concept for dynamical systems and has wide applications in geophysical fluid dynamics (GFD) (e.g., Holton, 1992; Cushman-Roisin, 1994; Pedlosky, 1979). Like any infinite dimensional dynamical process, GFD instabilities in nature are generally localized in space and time, in the sense that instabilities tend to occur episodically and within limited regions which may have irregular geometries and could be advected around. In the classical framework, however, stability is a notion over the whole system to which every location belongs. It is difficult to believe that such a bulk treatment can have the highly localized processes faithfully represented. This problem is not new. People have developed many approximate approaches for certain problems, which generally can be put into two categories: (1) Lagrangian; (2) Eulerian but linear. The former includes the well-known Lyapunov exponent technique (e.g. Wiggins, 2003), and the parcel stability analysis which has been utilized to investigate symmetric instability (see Holton, 1992, and references therein); the latter approach often uses the WKB expansion, and can be found, for example, in the study of absolutely and convectively unstable flows (e.g., Pierrehumbert and Swanson, 1995). Considering that a majority of GFD datasets are acquired in Eulerian form, and that instability processes are more often than not of finite amplitude, it is desirable to have a more generic formalism to integrate together localization and nonlinearity in an Eulerian framework.

We use the MS-EVA developed in LR1 to establish the formalism. MS-EVA is based on a mathematical machinery called multiscale window transform (MWT) which is introduced in LR1, Section 2, and in more detail in Liang (2002) and Liang and Anderson (2007). Like the WKB expansion used in the previous convective/absolute instability analysis, MWT is localized in nature; unlike WKB, the MS-EVA does not involve a small perturbation approximation. The MWT-based MS-EVA is therefore expected to serve our purpose well. Indeed, MS-EVA is closely tied to stability in that stability/instability belongs to a kind of energy transfer process between *scale windows*. A scale window, or simply a window, is a subspace involving a range of scales (refer to Liang and Anderson (2007) for a rigorous definition). In the classical sense, stability analysis deals with the behavior of perturbations to some equilibrium state of a system. This equilibrium state could be a time-invariant solution, a limit cycle, etc. Either way it can be put into a more abstract class—a large-scale (time) window with a proper window bound. Along this route stability/instability is naturally generalized as the interaction between time scale windows. We start from this point to conceptualize our problem and form the criteria for the identification of barotropic and baroclinic instabilities on a generic basis.

Our strategy is to connect certain MS-EVA terms to the classical definition, starting with a linear equation, then advancing in two steps. The first step is *nonlinearization*. We re-state, in the linear limit, the classical definition in MS-EVA language, and within that limit go to the nonlinear version. The resulting definition equation is now nonlinear but still global. At this time we move to the second step: *localization*. We will show, in terms of MWT and MS-EVA, what makes the definition global is reduced to two operators, a time marginalization (cf. LR1) and a spatial averaging. Localization is achieved through relaxing or freeing the equation from the constraints of these operators. Based on the relaxed equation a nonlinear localized instability analysis is then possible.

This paper is organized as follows. Sections 2 and 3 are devoted to realizing the above strategy. Instability criteria are then established and compared to the existing Eulerian formalisms (Section 4). In Sections 5.1 and 7, the criteria are validated with an Eady model (pure baroclinic instability), and a Kuo model (Section 5.2). We demonstrate that our localized instability analysis reduces to but extends the concept of Reynolds stress and yields a mean–eddy structure interaction consistent with Kuo's barotropic instability theorem. This section is followed by a brief description of the energetic scenario of baroclinic and barotropic instabilities (Section 6), and an exemplification of the analysis with a highly localized nonlinear instability problem (Section 7). Dynamical consistency is checked with the known results, and capabilities are shown in treating nonlinearity as well as temporal and spatial intermittence. This study is summarized in Section 8.

2. MS-EVA re-statement of the classical instability formalism

In this section, we re-state the classical instability problem using the MS-EVA language. This re-statement makes it possible for a direct generalization of the classical formalism, which we will show in Sections 3 and 4.

2.1. Classical linearized formalism

In the classical formalism, the two important concepts, baroclinic instability and barotropic instability, can be defined in the context of the linearized growth equation of perturbation energy

$$E_{\text{eddy}} = \frac{1}{2}\overline{\underline{\mathbf{v}}' \cdot \underline{\mathbf{v}}'} + \frac{1}{2}c\overline{\rho'^2}, \qquad \text{where } c = \frac{g^2}{\rho_0^2 N^2},$$

for a frictionless and nondiffusive zonal jet stream over a basin Ω (Pedlosky, 1979; Holton, 1992; Cushman-Roisin, 1994)[1]:

$$\frac{\partial \langle E_{\text{eddy}} \rangle^{\Omega}}{\partial t} = \left\langle -c\overline{v'\rho'}\frac{\partial \bar{\rho}}{\partial y} - c\overline{w'\rho'}\frac{\partial \bar{\rho}}{\partial z} \right\rangle^{\Omega} + \left\langle -\overline{u'v'}\frac{\partial \bar{u}}{\partial y} - \overline{u'w'}\frac{\partial \bar{u}}{\partial z} \right\rangle^{\Omega}$$

$$\equiv \langle \text{BC}^* \rangle^{\Omega} + \langle \text{BT}^* \rangle^{\Omega}. \tag{1}$$

In the equation, ρ is the density anomaly defined such that the total density

$$\rho_{\text{total}} = \rho_0 + \tilde{\rho}(z) + \rho,$$

---

[1] In this equation, the term $\overline{u'w'}(\partial \bar{u}/\partial z)$ in BT* and the term $c\overline{w'\rho'}(\partial \bar{\rho}/\partial z)$ in BC* are not seen in typical textbooks where a quasi-geostrophic (QG) flow is usually assumed. In primitive equation models, these terms could be significant.

where $\rho_0 = \text{const}$ (say 1025), $\tilde{\rho}(z)$ is equal to $(\rho_{\text{total}} - \rho_0)$ averaged over the whole x–y plane and the time duration, and $N^2 = -(g/\rho_0)(d\tilde{\rho}/dz)$. The angle bracket $\langle \cdot \rangle^\Omega$ is an averaging over Ω confined between two latitudes; the overbar stands for an ensemble mean which is practically replaced by a time average,[2] and the prime for the departure from it. Other symbols are conventional (refer to the textbooks cited above). In this formalism, the two types of instabilities are distinguished by the contributions of $\langle BC^* \rangle^\Omega$ and $\langle BT^* \rangle^\Omega$. For convenience, we will loosely refer to them as baroclinic transfer and barotropic transfer, respectively.

One may encounter difficulty when applying the theory of stability/instability based on (1) to the studies of real ocean and atmosphere processes, which are in general highly nonlinear and intermittent in space and time. The problem arises from the averages, the overbars and the angle brackets. One naturally wonders why they cannot be removed to obtain a more faithful formulation. The reason is as follows. The overbars are applied for the multiscale decomposition; without them there is no way to talk about multiscale energetics and hence stability/instability. The spatial averages (represented by angle brackets) serve to average out the transport processes to have the mean–eddy transfers stand out. This is important, as BC^* and BT^* contain not just transfers, but also transports which are irrelevant to hydrodynamic stability. To see why, consider a barotropic flow. Its mean and eddy kinetic energy equations in the classical sense are (cf. LR1)

$$\frac{\partial K_{\text{mean}}}{\partial t} + \nabla \cdot \underline{\mathbf{Q}}_{\text{mean}} = -(\nabla \cdot \overline{\mathbf{v}'\mathbf{v}'}) \cdot \bar{\mathbf{v}}, \tag{2}$$

$$\frac{\partial K_{\text{eddy}}}{\partial t} + \nabla \cdot \underline{\mathbf{Q}}_{\text{eddy}} = -\overline{\mathbf{v}'\mathbf{v}'} : \nabla\bar{\mathbf{v}}, \tag{3}$$

where the two $\mathbf{Q}$ terms stand for some fluxes (including pressure work) which are not helpful for the illustration. Observe that the right hand side of (3) is BT^*; it does not cancel the right hand side of (2). This is not what one expects of a transfer, as physically a transfer process should be a redistribution of energy among scales, without generating or destroying energy as a whole. BT^* hence does not define a barotropic stability/instability. Likewise, BC^* does not define a baroclinic stability/instability, either. So the spatial averages cannot be removed from (1).

Though not successful, the relaxation of the averaging operators in (1) offers a clue to a more flexible and faithful formulation for the geophysical fluid flow instabilities. As will be seen soon, this is made possible within our MS-EVA framework.

2.2. *Eddy window and energetics on the eddy window*

As argued above, the right hand side of (1) represents a kind of energy transfers between the mean and the eddy processes. It should be connected to our perfect transfers, namely, transfers with total energy conserved, that are established in LR1. To see more clearly this connection, we take a direct sum of two subspaces (in the context of time), the mesoscale and sub-mesoscale windows as introduced in LR1, to make an *eddy window*, and examine the energetics for this window.

---

[2] In many standard problems the ensemble mean may be replaced by a zonal average. We do not consider this case in order to connect (1) to the time scale window-based MS-EVA equations.

Table 1
Symbols for multiscale energetics (location n, window ϖ)

Kinetic energy (KE)		Available potential energy (APE)	
$\dot{K}_n^{\varpi}$	Time rate of change of KE	$\dot{A}_n^{\varpi}$	Time rate of change of APE
$\Delta Q_{K_n^{\varpi}}$	KE advective working rate	$\Delta Q_{A_n^{\varpi}}$	APE advective working rate
$T_{K_n^{\varpi},h}$	KE transfer due to horizontal flow	$T_{A_n^{\varpi},\partial_h\rho}$	APE transfer due to hor. grad. of ρ
$T_{K_n^{\varpi},z}$	KE transfer due to vertical flow	$T_{A_n^{\varpi},\partial_z\rho}$	APE transfer due to ver. grad. of ρ
$-b_n^{\varpi}$	Rate of buoyancy conversion	b_n^{ϖ}	Rate of inverse buoyancy conversion
$\Delta Q_{P_n^{\varpi}}$	Pressure working rate	$TS_{A_n^{\varpi}}$	Imperfect APE transfer due to $(\partial\bar{\rho}/\partial z)$

Consider an ideal fluid flow. From LR1, the growths of kinetic energy (K_n^1) and available potential energy (A_n^1) on the eddy window (denoted by superscript 1) at time step n,

$$K_n^1 = \frac{1}{2}\hat{\underline{\mathbf{v}}}_n^{\sim 1} \cdot \hat{\underline{\mathbf{v}}}_n^{\sim 1}, \qquad A_n^1 = \frac{1}{2}c(\hat{\rho}_n^{\sim 1})^2,$$

[c the same as that in (1)][3] are governed by

$$\dot{K}_n^1 = \Delta Q_{K_n^1} + \Delta Q_{P_n^1} + T_{K_n^1} - b_n^1, \tag{4}$$

$$\dot{A}_n^1 = \Delta Q_{A_n^1} + T_{A_n^1} + b_n^1, \tag{5}$$

where the divergent form Q-terms represent transport processes, and the T-terms are the perfect transfers:

$$
\begin{aligned}
T_{K_n^1} &= T_{K_n^1,h} + T_{K_n^1,z} \\
&= -\hat{\underline{\mathbf{v}}}_n^{\sim 1} \cdot \nabla \cdot (\widehat{\mathbf{v}\underline{\mathbf{v}}})_n^{\sim 1} + \nabla \cdot [(\widehat{\mathbf{v}\underline{\mathbf{v}}})_n^{\sim 1} \cdot \hat{\underline{\mathbf{v}}}_n^{\sim 1}] - \hat{\underline{\mathbf{v}}}_n^{\sim 1} \cdot \frac{\partial}{\partial z}(\widehat{w\underline{\mathbf{v}}})_n^{\sim 1} + \frac{\partial}{\partial z}[\hat{\underline{\mathbf{v}}}_n^{\sim 1} \cdot (\widehat{w\underline{\mathbf{v}}})_n^{\sim 1}],
\end{aligned}
\tag{6}
$$

$$
\begin{aligned}
T_{A_n^1} &= T_{A_n^1,\partial_h\rho} + T_{A_n^1,\partial_z\rho} + TS_{A_n^1} \\
&= -\frac{g^2}{\rho_0^2 N^2}\hat{\rho}_n^{\sim 1}\left[\nabla \cdot (\widehat{\rho\mathbf{v}})_n^{\sim 1} + \frac{\partial}{\partial z}(\widehat{w\rho})_n^{\sim 1}\right] \\
&\quad + \frac{g^2}{\rho_0^2 N^2}\left[\nabla \cdot (\hat{\rho}_n^{\sim 1}(\widehat{\rho\mathbf{v}})_n^{\sim 1}) + \frac{\partial}{\partial z}(\hat{\rho}_n^{\sim 1}(\widehat{w\rho})_n^{\sim 1})\right].
\end{aligned}
\tag{7}
$$

In the equations, the symbol $(\hat{\cdot})_n^{\sim 1}$ indicates an eddy window transform at time step n. Other notations are defined in LR1, and Table 1.

The T-terms in (4) and (5) represent energy transfers toward the eddy window. They are expected to be related to the $\langle BC^*\rangle^\Omega$ and $\langle BT^*\rangle^\Omega$ in Eq. (1). This is indeed true, as we hereafter prove.

---

[3] A constant transform factor is omitted for succinctness; see LR1, Section 3.2.

2.3. Barotropic transfer

As shown in LR1, Section 8, the connection between the classical energetics analysis and the MS-EVA is established through marginalization, which is a special summation over the time sampling space (see LR1, Section 2.3, and Liang and Anderson, 2007, for details). Similarly, we need to perform marginalization here. We need particularly to focus on the case with a large-scale window bound $j_0 = 0$ and a periodic extension, where the large-scale and eddy window syntheses reduce to duration average and the departure from it. That is to say,

$$q^{\sim 0} = \bar{q}, \qquad q^{\sim 1} = q'.$$

This allows us to write the marginalization property simply as

$$\mathcal{M}_n \hat{p}_n^{\sim 1} \hat{q}_n^{\sim 1} = \overline{p'q'}, \tag{8}$$

where $\mathcal{M}_n$ stands for the marginalization over all time steps. To see how $\langle \mathrm{BT}^* \rangle^{\Omega}$ is related to (4), marginalize $T_{K_n^1}$:

$$\mathcal{M}_n T_{K_n^1} = \mathcal{M}_n(T_{K_n^1,h} + T_{K_n^1,z}) = \mathcal{M}_n \left[-\hat{\mathbf{v}}_n^{\sim 1} \cdot \nabla \cdot (\widehat{\mathbf{v}\,\mathbf{v}})_n^{\sim 1} - \hat{\mathbf{v}}_n^{\sim 1} \cdot \frac{\partial}{\partial z}(\widehat{w\mathbf{v}})_n^{\sim 1} - \Delta Q_{K_n^1} \right]$$

$$= -\overline{\mathbf{v}' \cdot \nabla \cdot (\mathbf{v}\,\mathbf{v})'} - \overline{\mathbf{v}' \cdot \frac{\partial}{\partial z}(w\mathbf{v})'} + [\text{other}']. \tag{9}$$

The term [other$'$] is in a divergence form. It integrates to zero given the boundary conditions. So

$$\int \int \int_{\Omega} \mathcal{M}_n T_{K_n^1} \, \mathrm{d}V = -\int \int \int_{\Omega} \left[\overline{\mathbf{v}' \cdot \nabla \cdot (\mathbf{v}\,\mathbf{v})'} + \overline{\mathbf{v}' \cdot \frac{\partial}{\partial z}(w)'} \right] \, \mathrm{d}V$$

$$= -\int \int \int_{\Omega} \overline{u'v'} \frac{\partial \bar{u}}{\partial y} \, \mathrm{d}V - \int \int \int_{\Omega} \overline{u'w'} \frac{\partial \bar{u}}{\partial z} \, \mathrm{d}V \tag{10}$$

with the background field $\bar{\mathbf{v}} = (\bar{u}(y, z), 0, 0)$. In the derivation the continuity equation has been used and the triple perturbation terms have been dropped by linearization. This is to say, $\langle \mathrm{BT}^* \rangle^{\Omega}$ is equal to the marginalized total kinetic energy transfer (linearized) from the basic flow to the eddy window, i.e.,

$$\langle \mathcal{M}_n T_{K_n^1,h} + \mathcal{M}_n T_{K_n^1,z} \rangle^{\Omega} = \left\langle -\overline{u'v'} \frac{\partial \bar{u}}{\partial y} - \overline{u'w'} \frac{\partial \bar{u}}{\partial z} \right\rangle^{\Omega} = \langle \mathrm{BT}^* \rangle^{\Omega}. \tag{11}$$

2.4. Baroclinic transfer

We proceed to show that $\langle T_{A_n^1} \rangle^{\Omega} = \langle \mathrm{BC}^* \rangle^{\Omega}$. In Eq. (5), since the transport integrates to zero over the closed basin Ω, we need only consider the sum of

$$-c\hat{\rho}_n^{\sim 1} \nabla \cdot (\widehat{\rho \mathbf{v}})_n^{\sim 1} - c\hat{\rho}_n^{\sim 1} \frac{\partial}{\partial z}(\widehat{w\rho})_n^{\sim 1}$$

over all the possible n's. By the marginalization equality, this is

$$\mathcal{M}_n T_{A_n^{\varpi}} = -\overline{c\rho' \nabla \cdot (\rho \mathbf{v})'} - \overline{c\rho' \frac{\partial}{\partial z}(w\rho)'}.$$

Integrating, the first part becomes, with terms of higher order dropped (linearization),

$$\int \int \int_\Omega -\overline{c\rho' \nabla \cdot (\rho \underline{\mathbf{v}})'} \, dV = \int \int \int_\Omega c\bar{\rho}\overline{\rho' \frac{\partial w'}{\partial z}} \, dV - \int \int \int_\Omega c\frac{\partial \bar{\rho}}{\partial y}\overline{\rho' v'} \, dV.$$

The second part is

$$\int \int \int_\Omega -c\overline{\rho' \frac{\partial}{\partial z}(w\rho)'} \, dV = -\int \int \int c\overline{\rho' \frac{\partial}{\partial z}(w'\bar{\rho})} \, dV$$

$$= -\int \int \int_\Omega c\bar{\rho}\overline{\rho' \frac{\partial w'}{\partial z}} \, dV - \int \int \int_\Omega c\overline{\rho' w'} \frac{\partial \bar{\rho}}{\partial z} \, dV.$$

These two integrals sum to $-\int \int \int_\Omega (c(\partial\bar{\rho}/\partial y)\overline{\rho' v'} + c(\partial\bar{\rho}/\partial z)\overline{\rho' w'}) \, dV$, which is none other than the BC* integrated over Ω, i.e.,

$$\mathcal{M}_n \langle T_{A_n^1, \partial_h \rho} + T_{A_n^1, \partial_z \rho} + TS_{A_n^1} \rangle^\Omega = \langle BC^* \rangle^\Omega. \tag{12}$$

2.5. Re-statement of the classical formulation

Now return to Eq. (1). The right hand side has been expressed in MS-EVA terminology. On the left hand side, E_{eddy} is a sum of $K_{\text{eddy}} = (1/2)\overline{\underline{\mathbf{v}}' \cdot \underline{\mathbf{v}}'}$ and $A_{\text{eddy}} = (1/2)c\overline{\rho'^2}$. It is equal to the marginalization of $K_n^1 + A_n^1 \equiv E_n^1$, a direct result of the marginalization property of multiscale window transform. With these, Eq. (1) now can be written as

$$\mathcal{M}_n \langle \hat{\delta}_n E_n^1 \rangle^\Omega = \mathcal{M}_n \langle T_{A_n^1} + T_{K_n^1} \rangle^\Omega$$

$$= \mathcal{M}_n \langle T_{A_n^1, \partial_h \rho} + T_{A_n^1, \partial_z \rho} + TS_{A_n^1} \rangle^\Omega + \mathcal{M}_n \langle T_{K_n^1, h} + T_{K_n^1, z} \rangle^\Omega. \tag{13}$$

Here the time derivative has been modified as we did in deriving the multiscale energetic equations in LR1. Eq. (13) is open to the possibility of localization, which we will show next.

3. Toward the localized formalism

The strategy to formulate the localized instability analysis is to relax the constraints exerted by the "global" operators, i.e., the marginalization and the domain averaging, applied on Eq. (13). We will soon see, this is in general not trivial.

3.1. Relaxation of the spatial averaging

Relaxation of the angle averaging in Eq. (13) gives,

$$\mathcal{M}_n \dot{E}_n^1 = \mathcal{M}_n (T_{A_n^1} + T_{K_n^1}) + \mathcal{M}_n \nabla \cdot \underline{\mathbf{G}}_n, \tag{14}$$

where $\dot{E}_n^1 \equiv \hat{\delta}_n(A_n^1 + K_n^1)$, and $\nabla \cdot \underline{\mathbf{G}}_n$ is an arbitrary term in some divergence form. This is to say, the relaxation is unique up to a transport process. The key of spatial localization is therefore to have the transfer and transport separated. In LR1, we have shown that the separation can be achieved precisely through introducing the concept *perfect transfer*. By definition a perfect transfer T_n^ϖ is a process such that $\mathcal{M}_n \sum_\varpi T_n^\varpi = 0$. It is a redistribution of energy among scale

windows which does not generate nor destroy energy as a whole. In arriving at (14), we need to assure that $(T_{A_n^1} + T_{K_n^1})$ is perfect.

It should be pointed out that Eq. (13), and hence Eq. (1), are conditioned on the closed boundary configuration. Relaxation of the spatial averaging basically relieves this constraint and hence allows for a more flexible formulation.

3.2. Relaxation of the time marginalization

In order to drop the marginalization, we need to prove an equality which relates linearized transfers to interaction analysis.

For field variables $\mathcal{R}$, p and q, consider a basic transfer function

$$T(\varpi, n) = \hat{\mathcal{R}}_n^{\sim\varpi} \cdot (\widehat{pq})_n^{\sim\varpi}.$$

Here $\hat{\mathcal{R}}_n^{\sim\varpi}$ represents the multiscale window transform (MWT) of $\mathcal{R}$ on window ϖ and location n. Considering only the eddy window, $\varpi = 1$, the interaction analysis of $T(1, n)$ is, according to LR1 (Section 9),

$$T(1, n) = T_n^{0\to1} + T_n^{1\to1} = T_n^{0\to1} + \hat{\mathcal{R}}_n^{\sim1} \cdot (\widehat{p^{\sim1}q^{\sim1}})_n^{\sim1}, \tag{15}$$

where $0 \to 1$ and $1 \to 1$ stand for the directions of energy transfer ("mean to eddy" and "eddy to eddy", respectively), and $q^{\sim1}$ is the eddy window synthesis of q. Recall when $j_0 = 0$ and a periodic extension is adopted, $q^{\sim0} = \bar{q}$ and $q^{\sim1} = q'$, and $\mathcal{M}_n \hat{p}_n^{\sim1} \hat{q}_n^{\sim1} = \overline{p'q'}$. Applying $\mathcal{M}_n$ to both sides of (15), we get

$$\mathcal{M}_n T(1, n) = \mathcal{M}_n T_n^{0\to1} + \overline{\mathcal{R}' \cdot (p'q')'} = \mathcal{M}_n T_n^{0\to1} + \overline{\mathcal{R}' \cdot (p'q' - \overline{p'q'})}$$
$$= \mathcal{M}_n T_n^{0\to1} + \overline{\mathcal{R}' p'q'} \approx \mathcal{M}_n T_n^{0\to1} \quad \text{by linearization,}$$

or

$$\mathcal{M}_n T_n^{1\to1} = 0. \tag{16}$$

Eq. (16) expresses the linearization assumption in the MS-EVA framework.

The equality (16) allows for a relaxation of the marginalization on both sides of Eq. (14):

$$\dot{E}_n^1 = T_{A_n^1} + T_{K_n^1} + \nabla \cdot \underline{\mathbf{G}}_n + R_n^{1\to1}. \tag{17}$$

That is to say the relaxation is unique up to an arbitrary eddy window–eddy window transfer process $R_n^{1\to1}$ (cf. LR1, Section 9). A physically consistent choice is that $R_n^{1\to1} = -(T_{A_n^1}^{1\to1} + T_{K_n^1}^{1\to1})$, which yields

$$\dot{E}_n^1 = T_{A_n^1}^{0\to1} + T_{K_n^1}^{0\to1} + \nabla \cdot \underline{\mathbf{G}}_n. \tag{18}$$

This is the classical instability definition with the global operator constraints relaxed.

4. Nonlinear localized instability analysis

4.1. Criterion for instability identification

We proceed to build our localized instability analysis. This is a direct generalization of (1) from (18). Relaxed from marginalization and domain averaging, Eq. (18) is localized, both in space and in time. It verifies (1) under the assumptions of linearity and time decomposition with the gravest scale level index ($j_0 = 0$) and a periodic extension. The equation itself, however, does not have these limitations embedded. We define the localized instability analysis on the basis of this equation, and it therefore can be used for problems with finite perturbation and arbitrary window partitioning, i.e., the basic field is not necessarily an equilibrium, but could be any time-varying process.

A conspicuous difference between (18) and (1), except the time and space localization, is the relaxation "constant"—the additional transport. Because of this term, the time rate of change of eddy energy alone is no longer the instability indicator, as $\partial_t \langle E_{\mathrm{eddy}} \rangle^\Omega$ is in (1). This is to say, the disturbance could grow at a location even though no instability occurs. The necessary energy to fuel the growth could be transported from other places in the physical space.

In this spirit we formulate our analysis. Let

$$\mathrm{BT} = T_{K_n^1}^{0\to 1} = T_{K_n^1,h}^{0\to 1} + T_{K_n^1,z}^{0\to 1}, \qquad \mathrm{BC} = T_{A_n^1}^{0\to 1} = T_{A_n^1,\partial_h \rho}^{0\to 1} + T_{A_n^1,\partial_z \rho}^{0\to 1} + TS_{A_n^1}^{0\to 1}$$

with BT and BC (location index n suppressed for clarity) corresponding, respectively to their starred counterparts in (1). Here BT and BC are localized both in space and in time. We claim that they are just the two metrics for the localized barotropic instability and baroclinic instability. Considering that the concept of stability concerns a subsystem within its correlation scale, we apply a local spatial averaging on these two metrics. We will still use the notation $\langle \cdot \rangle^\Omega$ to write them as $\langle \mathrm{BT} \rangle^\Omega$ and $\langle \mathrm{BC} \rangle^\Omega$, but here $\langle \cdot \rangle^\Omega$ carries with a different meaning—it is an averaging over some appropriately chosen local region Ω. In this way an instability analysis in a localized sense is now possible. From Eq. (18):

(1) A subsystem is unstable if $\langle \mathrm{BT} + \mathrm{BC} \rangle^\Omega > 0$ and vice versa;
(2) For an unstable system, if $\langle \mathrm{BT} \rangle^\Omega > 0$ and $\langle \mathrm{BC} \rangle^\Omega \le 0$, the instability the subsystem undergoes is barotropic;
(3) For an unstable subsystem, if $\langle \mathrm{BC} \rangle^\Omega$ is positive but $\langle \mathrm{BT} \rangle^\Omega$ is not, then the instability is baroclinic;
(4) If both $\langle \mathrm{BT} \rangle^\Omega$ and $\langle \mathrm{BC} \rangle^\Omega$ are positive, the subsystem is undergoing a mixed instability.

It should be pointed out that the averaging $\langle \cdot \rangle^\Omega$ over an appropriate domain Ω is generally difficult to realize. In a highly idealized model (as the ones we will consider next), this might be not a difficult business; in real problems, however, an unambiguous choice of Ω is usually not feasible. We fix this problem with a *localized averaging*, which does not rely upon the choice of Ω—in fact, no Ω is necessary at all. This is achieved by a large-scale window synthesis (see Liang and Anderson, 2007) in the spatial direction with a proper window bound. Recall in eliminating the phase oscillation associated with the energetics (Section 3.5 of LR1), we have used the same technique.

4.2. Comparison with the previous formalisms

Our formulation begins with the classical definition, but the generalized localized stability analysis envisions stability problems differently than the classical formalism [cf. (1)] does. Instead of taking the whole system just as one object, it quantifies the energy transfer with a *field-like* function over a discretized form of that field. In other words, what characterizes the instability is a temporal-spatial structure, rather than a norm – a single positive value – as in the classical formalism. One can tell from the structure whether there is and where there is an instability without referencing the boundaries of the problem, and is hence of particular use for open flow problems. Our formalism is hence capable of coping with more realistic GFD problems.

Our formalism also differs from the previous localized Eulerian formalism, which relies on the approximation of small perturbation and, in most cases, a slowly and regularly varying (e.g., sinusoidal) background field. Our analysis is based on numerical results or experimental data, which can be made free of any approximation. The basic field could be of arbitrary shape, and the perturbation could be of finite amplitude. The capability of dealing with highly localized and finite amplitude events will be evidenced in Section 7.

Besides the above, a fundamental point which is distinctly different from all the previous formalisms lies at the transport-transfer separation performed in the formulation. When a special decomposition with $j_0 = 0$ and a periodic extension is chosen, the MS-EVA counterparts of (2) and (3) are (cf. LR1, Section 8, for derivation)

$$\frac{\partial K_{\text{mean}}}{\partial t} + \nabla \cdot \left(\underline{\mathbf{Q}}_{\text{mean}} + \frac{1}{2} \overline{\mathbf{v}'\mathbf{v}'} \cdot \bar{\mathbf{v}} \right) = -\text{BT}, \tag{19}$$

$$\frac{\partial K_{\text{eddy}}}{\partial t} + \nabla \cdot \left(\underline{\mathbf{Q}}_{\text{eddy}} + \frac{1}{2} \overline{\mathbf{v}'\mathbf{v}'} \cdot \bar{\mathbf{v}} \right) = \text{BT}, \tag{20}$$

where

$$\text{BT} = \frac{1}{2} \{ [\nabla \cdot (\overline{\mathbf{v}'\mathbf{v}'})] \cdot \bar{\mathbf{v}} - (\overline{\mathbf{v}'\mathbf{v}'}) : \nabla \bar{\mathbf{v}} \}. \tag{21}$$

Similarly, in this particular case, the baroclinic transfer is reduced to

$$\text{BC} = \frac{c}{2} \{ \bar{\rho} \nabla \cdot (\overline{\mathbf{v}'\rho'}) - \overline{\mathbf{v}'\rho'} \cdot \nabla \bar{\rho} \} \tag{22}$$

with $c = g^2/(\rho_0^2 N^2)$.

The difference between the above pair and the pair of (2)–(3) is easily seen. It may be better illustrated with a simpler basic flow through making contacts with Reynolds stress, a concept which has long been used to interpret the interaction between mean and eddy structures. It has been a convention to calculate the energy extracted by Reynolds stress against the basic profile, and take it as the indicator of instability [refer to the second term in Eq. (1)]. In the case of a basic flow $(\bar{u}(y), 0)$, for example, people usually calculate the quantity $-(\overline{u'v'})(\partial \bar{u}/\partial y)$ (cf. Tennekes and Lumley, 1972; Harrison and Robinson, 1978). In our formalism, the barotropic transfer BT is $(1/2)[\bar{u}\nabla \cdot (\overline{\mathbf{v}'u'}) - (\overline{u'v'})(\partial \bar{u}/\partial y)]$. Note the second term in the bracket is just the Reynolds stress contribution, but as shown in LR1, this term alone does not conserve energy over scale windows (i.e., the transfer expressed this way is *not perfect* in our language). Term $\bar{u}\nabla \cdot (\overline{\mathbf{v}'u'})$, together with the factor 1/2, should be included to ensure this conservation. The addition of this term makes the transfer mechanism usually quite different from that of $-(\overline{u'v'})(\partial \bar{u}/\partial y)$ alone.

Later on in Section 5.2.2(cf. Figs. 5 and 6), we will have a chance to see an example about the difference.

A direct consequence of the transport-transfer separation is that growth of perturbation energy does not necessarily mean instability. This is remarkable as it has been conventional to read instability by looking at the perturbation bursts from simulations. Think about a disturbance at some location: It may grow even without invoking any instability, as the energy needed to fuel its growth could be transported from surrounding regions. This is a fundamental property of infinite dimensional systems which is lacked in systems of low dimensionality. We will see later in the validations that this is generic in GFD flows, and our formalism has it naturally represented.

5. Validations

In this section, the benchmark Eady model is examined for the verification of our formalism. Also examined is a barotropic model which we use to check the dynamical consistency with Kuo's theorems on barotropic instability (Kuo, 1973). We want to demonstrate through this model that our analysis is able to yield a faithful mean–eddy structure interaction which is not seen with previous formalisms.

5.1. Consistency with the Eady model

The Eady model is among one of the most extensively studied examples of linear stability. Introduced by Eady (1949) in an simple form, it has since become a benchmark for baroclinic instability studies. Recently, it was even shown that the linear instability criterion also works in the presence of nonlinearity (Mu and Shepherd, 1994; Liu and Mu, 1996), a remarkable result adding more elegance to the model. In the following, we use an unstable mode to verify that $\langle BC \rangle^{\Omega}$ is positive, and $\langle BT \rangle^{\Omega} = 0$; and a stable mode to verify that both $\langle BC \rangle^{\Omega}$ and $\langle BT \rangle^{\Omega}$ are vanish.

Appendix A gives a summary of the Eady solution. Based on it, a stable mode and an unstable mode are selected to generate two datasets for our purpose. The numbers and other details are referred to the appendix. We here only need a qualitative description.

For the unstable mode, both BC and BT vary in z and oscillate in x. Their horizontal oscillations, however, are fundamentally different. A plot of these transfer rates as functions of x for the mid-depth (450 m) is shown in Fig. 1. From it we see that BC actually does not oscillate around the zero. It favors positive values, in contrast to BT, which has negative and positive values well balanced. If averaged over a wavelength, there is a net gain in BC, while BT vanishes. This trend holds for all the levels throughout the water column. If we use $\langle \cdot \rangle^{xy}$ to indicate horizontal averaging (over integer wavelengths), then $\langle BC + BT \rangle^{xy} > 0$. By the criteria established in Section 4, the system is dynamically unstable. Moreover, $\langle BC \rangle^{xy} > 0$ and $\langle BT \rangle^{xy} = 0$, implying that the instability is purely baroclinic, exactly as we expect.

We extend the validation to the stable and neutrally stable datasets. The energetic patterns (figures not shown) are fairly symmetric, and the unstable scenario described before is not seen. Both BT and BC average to nil in these cases.

A fundamental aspect of our localized stability analysis which is distinctly different from its classical counterpart is that our stability/instability is not measured by a single norm over the domain and duration under concern; it generally has a field or spatio-temporal structure. For the unstable Eady mode, $\langle BC \rangle^{\Omega}$ is distributed uniformly in z (Fig. 2a), although in this case the horizontal flow increases with height (cf. Appendix A). This makes sense, as one might have
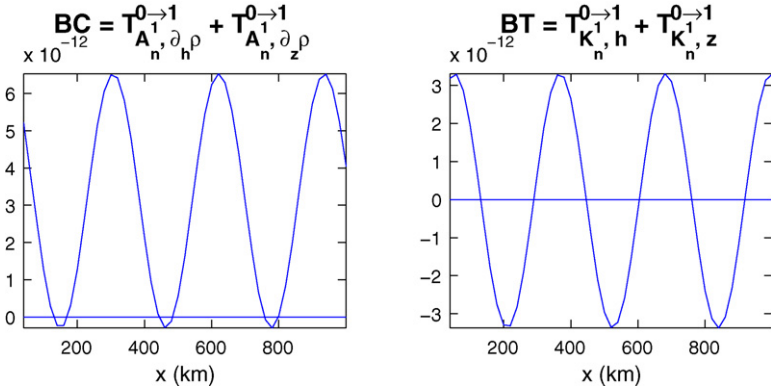
Fig. 1. Instability indicators BC $= T^{0\to1}_{A^1_n,\partial_h\rho} + T^{0\to1}_{A^1_n,\partial_z\rho} + TS^{0\to1}_{A^1_n}$ ($TS_{A^1_n} = 0$ here) and BT $= T^{0\to}_{K^1_n,h} + T^{0\to}_{K^1_n,z}$ as functions of x for the mid-depth (level 5) of the unstable Eady mode (cf. Appendix A).
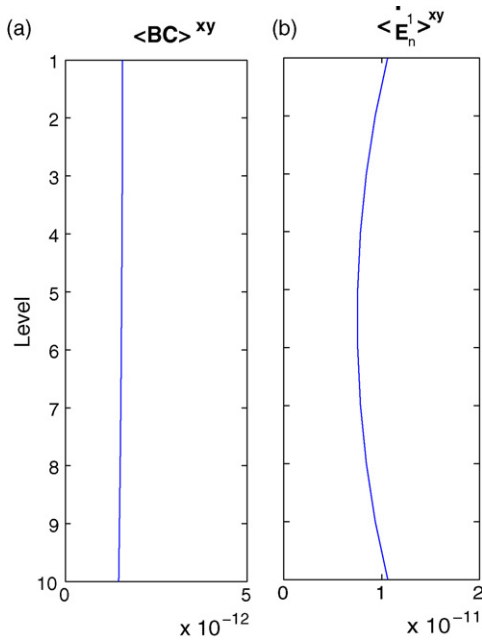

Fig. 2. Horizontally averaged BC (a) and time rate of change of eddy energy E^1_n (b) as functions of vertical levels. The symbol $\langle\cdot\rangle^{xy}$ indicates averaging over a wavelength on the x–y plane.

intuitively expected, considering the symmetric model configuration in z. The uniform BC differs from the time rate of change of total eddy energy, $\dot{E}^1_n$, which maximizes at the two boundaries (Fig. 2b).[4] As it has been conventional to connect the growth of perturbation energy to instability, the discrepancy between BC and $\dot{E}^1_n$ is remarkable. The eddy energy growth might not be an

---

[4] The z-uniformity of BC is in agreement with the depth-independent structure of $-c\overline{v'\rho'}(\partial\bar{\rho}/\partial y)$, the eddy density transfer in the classical framework for an Eady wave.

Fig. 3. A sketch of the background velocity $\bar{u}(y)$ (a), and vorticity gradient $\bar{q}_y = -(\partial^2 \bar{u}/\partial y^2)$ (b) for the Kuo model. The five regimes resulting from this basic structure and the chosen phase speed c_r (see Appendix B) are indicated in (c).

appropriate indicator of instability. In Section 5.2 we will see a more dramatic example where energy transfer and time change of eddy energy could be qualitatively different.

5.2. Validation with a barotropic stability model

We still have one more criterion to validate: a system with a positive averaged BT and a zero (or negative) BC is barotropically unstable. In this section, we use Kuo's model (Kuo, 1949, 1973) to carry out this validation.

5.2.1. The model

Consider a barotropic (BC is hence zero) cosine zonal jet

$$\bar{u}(y) = \bar{u}_{max} \cos^2 \left(\frac{\pi}{2} \frac{y}{L} \right) \tag{23}$$

channeled between $y = \pm L$ (see Fig. 3a). It has an ambient potential vorticity gradient (Fig. 3b)

$$\bar{q}_y = -\bar{u}_{yy} = \frac{\pi^2}{2L^2} \bar{u}_{max} \cos \frac{\pi y}{L}, \tag{24}$$

which vanishes at $y = \pm(L/2)$, meeting the necessary condition for barotropic instability by Rayleigh's theorem.

The model result is summarized in Appendix B. We choose two particular modes to build the datasets for our validation. For the stable mode, the solution shows on the x–y domain a pattern symmetric about $x = 0$ and $y = 0$, while for the unstable mode, this symmetry breaks. An snapshot of the unstable perturbation velocity u' and v' is shown in Fig. 4, where a conspicuous feature is the kinky variation of u' with y (Fig. 4a). We will see soon that these kinks make the Kuo model a good testbed for our localized stability analysis.

5.2.2. Validation

According to Section 4, the barotropic instability indicator BT should average to a positive number for the unstable mode, and zero for the stable mode. This is true with the datasets generated above. The classical result is thereby recovered.
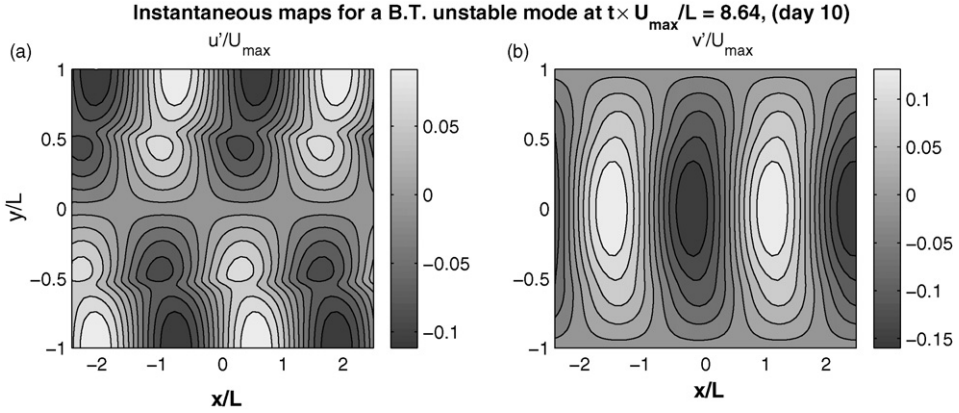
Fig. 4. A snapshot of u' (a) and v' (b) for the barotropically unstable mode ($kL = (3/4)\pi$). See Appendix B for explanation of parameters.

As BC in the Eady model case, here BT also displays some spatial variation which is not seen in a classical framework. We are particularly interested in its variation in y because of the meridionally structured basic configuration. Fig. 5a shows the x-averaged BT as function of y, where we see a bell shape of positive quantity in the middle. A conspicuous feature is that there are two sharp peaks with negative values at $y = \pm 0.53L$. That is to say, the flow is locally stable around those two points, even though as a whole the system is unstable!

The striking inverse transfer corresponds precisely in location to the kinky distribution of u' in Fig. 4. To see why there should be such a phenomenon, recall that for a barotropic instability to exist, it requires not only that a basic potential vorticity gradient $\bar{q}_y$ change sign through $y \in [-L, L]$, but also that $(\bar{u} - c_r)$ (c_r the mode phase speed) and $\bar{q}_y$ be positively correlated over the same domain (Kuo's theorem, as called by Pedlosky, 1979). (See Kuo, 1973, pp. 277–279.) Although this positive correlation requirement is stated in an integral form, locally (in y) it may apply wherever the system is more or less meridionally isolated. This is to say, the sign of the
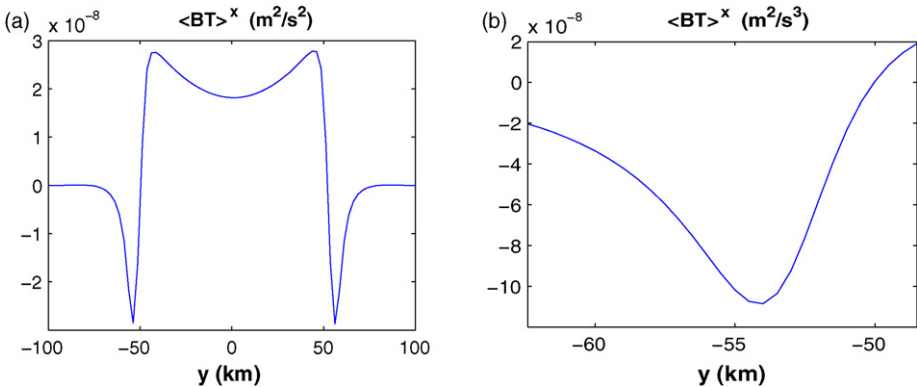

Fig. 5. A snapshot of the meridional distribution of the x-averaged BT for the unstable Kuo mode ($t = 10$ days). Notice the two sharp negative valleys. They correspond to the two narrow regimes in Fig. 3c. The BT has the same structure for all instants, except for a growing amplitude with time. (b) A close-up of (a) around $y = -0.53L$ with six times model resolution. Symbol $\langle \cdot \rangle^x$ signifies averaging over one wavelength in the zonal direction.
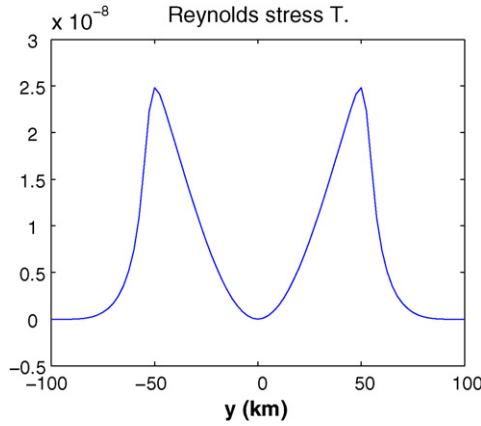
Fig. 6. Energy extracted by Reynolds stress against the basic flow profile $\langle -\overline{u'v'}(\partial \bar{u}/\partial y)\rangle^x$ (in m^2/s^2) for the unstable Kuo mode (averaged zonally over one wavelength). Notice the two positive peaks around ± 50 km (in contrast to the two sharp valleys of Fig. 5a).

product $(\bar{u} - c_r) \times \bar{q}_y$ may be pivotal to the instability, and hence the zero points of $\bar{u} - c_r$ and $\bar{q}_y$ are critical to the dynamics. In this chosen mode, $c_r = 0.4504\bar{u}_{\max}$, thus

$$\bar{u}(y) - c_r = 0 \Rightarrow y = \pm 0.53L, \tag{25}$$

$$\bar{q}_y = -\bar{u}_{yy} = 0 \Rightarrow y = \pm 0.50L. \tag{26}$$

These critical y's divide the flow into five regimes, as sketched in Fig. 3c. In the middle regime (hatched), both $\bar{q}_y$ and $\bar{u} - c_r$ are positive, so their product is also positive. The regimes at the two ends, with both $\bar{q}_y$ and $\bar{u} - c_r$ being negative, also have a positive product $\bar{q}_y(\bar{u} - c_r)$. These polar regimes and the interior regime are separated near $y = \pm 0.5L$ by two narrow strips (with a width of only $0.03L$) where $\bar{q}_y(\bar{u} - c_r) < 0$, and just because of the opposite sign of $\bar{q}_y(\bar{u} - c_r)$, the dynamics in the strips could be completely different from the interior regime. In this sense, our localized stability theory yields an instability structure consistent with the known dynamics.

The stable transfer embedded in the unstable field is interesting. If computed with a higher resolution, these inverse transfer peaks do not appear impulse-like. They actually have some y structures. As shown in Fig. 5b, the peaks do not really span only the critical bands ($0.5L$ to $0.53L$ and $-0.53L$ to $0.5L$). Rather, there is a tail extending beyond the $\pm 0.53L$ limits. This is in agreement with the above conjecture, as what Kuo's theorem states is in the form of an integral with respect to y from $-L$ to L, rather than a local one.

It has long been a convention to use the concept of Reynolds stress to interpret the mean–eddy interactions in a flow. We calculate the energy extracted by Reynolds stress against the basic profile, $\langle -\overline{u'v'}(\partial \bar{u}/\partial y)\rangle^x$, and plot it in Fig. 6. Observe that it does not correlate well, as $\langle BT \rangle^x$ in Fig. 5 does, to the distinct sharp configuration (Fig. 3c) demarcated by the background vorticity gradient and phase speed. Particularly, it vanishes in the middle, while predicting maximal positive transfer, or most unstable flow, at $\pm(L/2)$ (± 50 km in the plot), where Kuo's second necessary condition for instability is not met. This is in contrast to the pattern of $\langle BT \rangle^x$ in Fig. 5, which agrees well with Kuo's theorem. We are pleased to see that our analysis yields a dynamically consistent mean–eddy interaction which is not observed in the Reynolds stress framework.
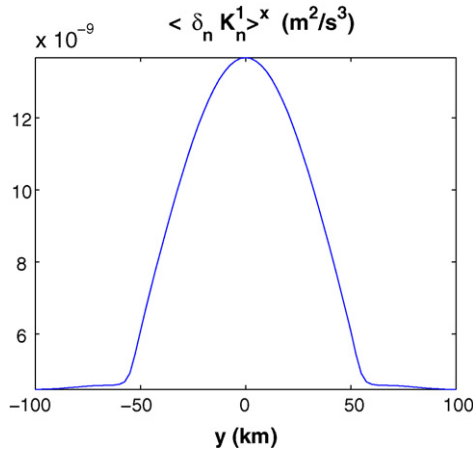
Fig. 7. Eddy energy growth rate (averaged zonally over one wavelength) $\langle \dot{K}_n^1 \rangle^x$ (in m^2/s^2) for the unstable Kuo mode.

It is also a convention to relate instability to perturbation burst. In general, however, perturbation growth does not seem to be an appropriate indicator. Plotted in Fig. 7 is the x-averaged time rate of change of eddy kinetic energy. Apparently, $\dot{K}_n^1$ does not correlate to BT well. Eddy energy grows everywhere through the latitudes, lacking a critical negative band as in the BT plot. This validation shows, inference of instability by simply looking at the perturbation from a simulation should be used with caution.

6. The aftermath of instabilities

The process after a system loses its instability is of interest in many problems. This section presents the energetic scenarios of a baroclinic instability and a barotropic instability with the unstable Eady and Kuo modes.

6.1. Eady mode

In an unstable Eady mode, both the density perturbation and velocity perturbation intensify toward the two vertical boundaries (e.g., Holton, 1992). The eddy energy distribution in Fig. 8a and b show this trend. A natural question is how this structure arises. We plot in Fig. 8c and d two MS-EVA terms: eddy-scale buoyancy conversion $\langle b_n^1 \rangle^{xy}$ and vertical pressure working rate $\langle \Delta_z Q_{P_n^1} \rangle^{xy}$. The negative $\langle b_n^1 \rangle^{xy}$ implies a steady conversion of eddy APE to eddy KE, which is carried away by the vertical pressure work because of the correlation between $\langle b_n^1 \rangle^{xy}$ and $\langle \Delta_z Q_{P_n^1} \rangle^{xy}$. The energetic scenario is now clear: Originally, there is no perturbation energy present and both $\langle A_n^1 \rangle^{xy}$ and $\langle K_n^1 \rangle^{xy}$ are zero. When a baroclinic instability occurs, a part of potential energy is released from the large-scale reservoir, directing toward the eddy window of APE. This release is achieved through the transfer process represented by $\langle BC \rangle^{xy}$, which is uniformly distributed through the water column. Due to this transfer, the eddy APE is increased accordingly. But the increase is different level by level, as there exists a sink for $\langle A_n^1 \rangle^{xy}$, the buoyancy conversion, which is minimal at the two boundaries and maximal in the middle. The buoyancy conversion carries the perturbation potential energy over the APE–KE bridge to activate
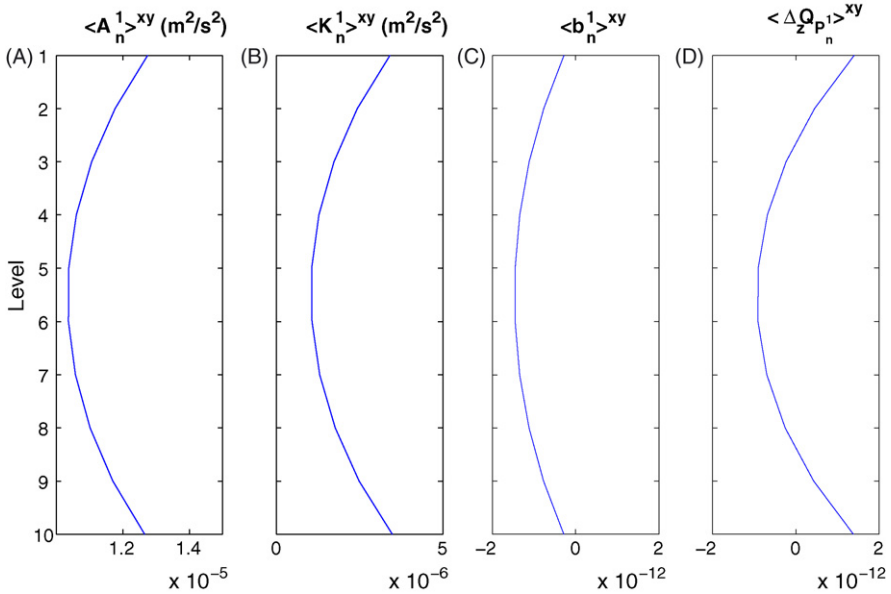
Fig. 8. Horizontally averaged energies $\langle A_n^1 \rangle^{xy}$ (a) and $\langle K_n^1 \rangle^{xy}$ (b) (in m²/s²), and energetic terms $\langle b_n^1 \rangle^{xy}$ (c), $\langle \Delta_z Q_{P_n^1} \rangle^{xy}$ (d) (in m²/s³).

the eddy motion. The converted energy would be piled up at the mid-depths, if not for the vertical pressure work $\langle \Delta_z Q_{P_n^1} \rangle^{xy}$. In response $\langle \Delta_z Q_{P_n^1} \rangle^{xy}$ ushers the converted eddy energy immediately upward and downward, as that in the QG–EVA scenario by Pinardi and Robinson (1986). The result of the process is simple. It ends up with two dumbbell-shape vertical profiles, for both the eddy available potential energy and kinetic energy (Fig. 8a and b). The whole process is pictorially presented in Fig. 9. The resulting vertical structure for either $\langle A_n^1 \rangle^{xy}$ or $\langle K_n^1 \rangle^{xy}$ implies that, when the instability halts, all the disturbances, either in horizontal velocity or in density, will be trapped near the two vertical boundaries, a pattern consistent with the known results. This is the general energetic scenario of Eady instability, which is some sense gives a validation of the MS-EVA.

6.2. Kuo mode

A remarkable feature of the unstable Kuo model is the negative transfer around the critical latitudes $y = \pm 0.5L$. This transfer is balanced by $\langle \Delta_y Q_{K_n^1} \rangle^x$, the meridional transport which is highly correlated to BT through the latitudes except for the opposite sign (figure not shown). Referring to Fig. 5, this correlation exhibits a clear energetic scenario for the Kuo model barotropic instability. The cartoon of Fig. 10 summarizes this scenario. The two narrow hatched regimes, where $(\bar{u} - c_r)\bar{q}_y < 0$, form the two "walls" of a well which limits the energetic activities. Before the system gets perturbed, K_n^1 (and hence $\langle K_n^1 \rangle^x$) is uniformly zero. When an instability sets up, a part of energy is transferred from the large-scale window to feed the growth. The transfer takes place only in the well, and the transferred energy due to this parietal process is transported from the center toward its two wings until it hits the walls where the poleward transportation is almost
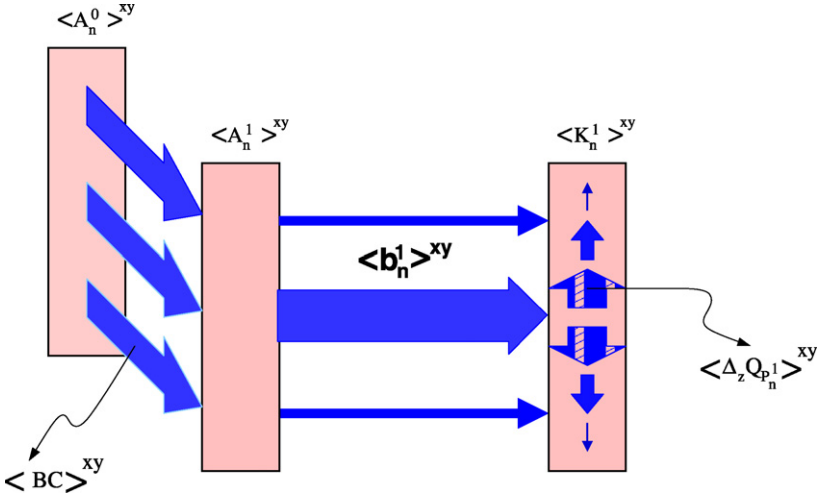
Fig. 9. A cartoon of the energetic scenario for the Eady-like baroclinic instability. When the instability happens, potential energy is transferred from the large-scale window toward the eddy window, and the measure of this transfer, $\langle BC \rangle^{xy}$ (the angle bracket represents an averaging over the x–y plane) is uniformly distributed in the vertical direction (middle row). At the same time, the eddy APE is converted to the eddy KE. The conversion is maximized at the middle depth, where the converted energy is brought upward and downward by the vertical pressure work ($\langle \Delta_z Q_{P_n^1} \rangle^{xy}$). The whole process results in two dumbbell-shape distributions of eddy potential energy and kinetic energy with depth (see Fig. 8).

halted (a very small part of transport still exists and that makes the K_n^1 increase, as shown in Fig. 7). An inverse transfer then brings the transported energy back to the large-scale window, effectively barring the perturbation from going further southward and northward. The final result is an equilibrium with a bell-shape distribution of eddy energy which is maximized at $y = 0$ and vanishes at the northern and southern ends.
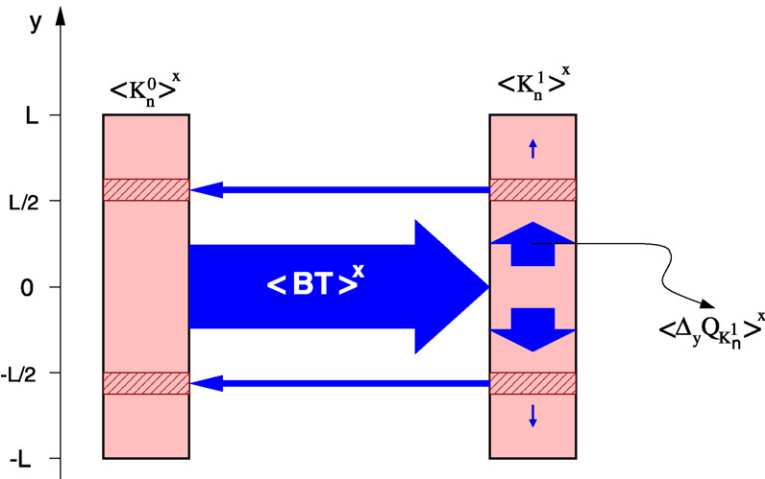

Fig. 10. A cartoon of the MS-EVA processes that make the Kuo barotropic instability. Hatched are the critical regimes where $(\bar{u} - c_r)\bar{q}_y < 0$.
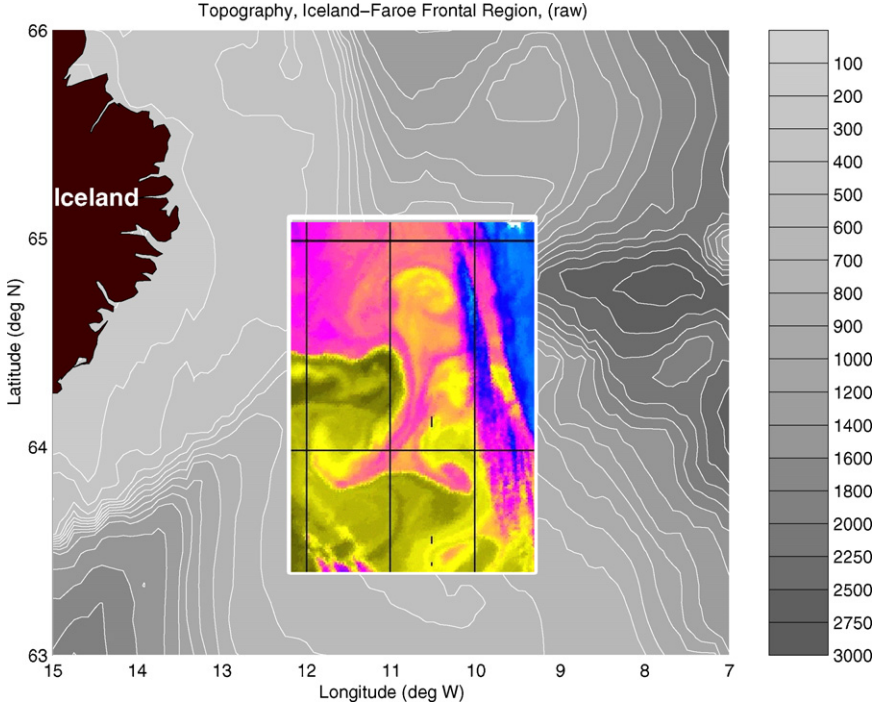
Fig. 11. Topography of the Iceland–Faeroe Front region. Inserted in the middle is the survey domain superimposed with a satellite image for the sea surface temperature on 22 August 1993.

7. Exemplification with a localized nonlinear Eady-like instability problem

The strength of our analysis lies in the study of highly localized and nonlinear processes. As we will show below, the meandering intrusion of the Iceland–Faeroe Front (IFF) is an ideal problem to demonstrate this strength.

The IFF is an oceanic front across the strait between Iceland and Faeroe Islands (Fig. 11). It forms a boundary separating the North Atlantic waters from the Arctic waters. In the August of 1993, an unprecedented dataset was obtained which captures the processes toward the formation of a highly localized meandering intrusion, as shown in Fig. 11 in the inserted satellite picture of sea surface temperature (SST) (Robinson et al., 1996). In this section, we briefly present part of the results relevant to this validation. For the whole story, the reader is referred to LR2.

The meandering intrusion is found to be associated with a localized nonlinear Eady-like baroclinic instability. Firstly, the intrusion is highly localized in space and time. On the SST image of 22 August 1993, it appears within a limited region in the middle of the model domain (Fig. 11). In the time direction, the intrusion occurred on an interval of approximately 2.6 days (see LR2; also cf. Fig. 12), with its geometry varying and the meandering center moving (figures not shown). Secondly, the intrusion is nonlinear. Its amplitude of variation is bounded in space and time, which is obvious both on the satellite image (Fig. 11) and in the time series (Fig. 12). Besides, the intrusion seems to be with a baroclinic instability, as evidenced by Miller et al. (1995).

The baroclinicity, nonlinearity, and localization makes the IFF an ideal testbed for our analysis. For this problem, it is expected to generate a locally positive BC and a negligible BT. This is indeed
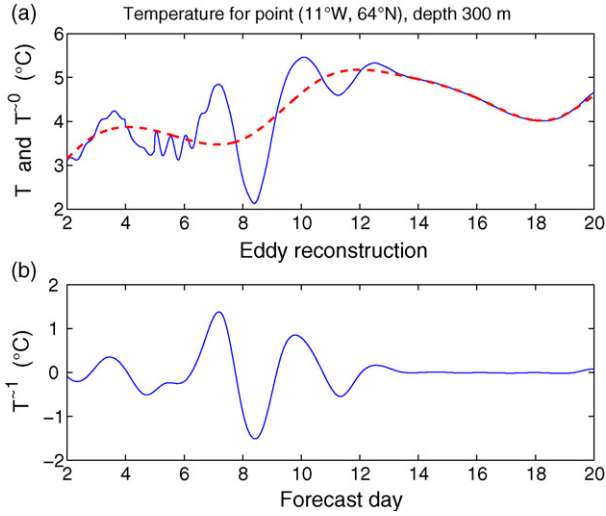
Fig. 12. A time series of the temperature (top, solid), and its large-scale window synthesis (top, dashed) and eddy window synthesis (bottom) for point (11°W, 64°N), depth 300 m. The decomposition is such that processes with periods shorter than and equal to 2.6 days (characteristic of the meandering intrusion) are included in the eddy window. In the bottom panel, signals with periods shorter than 0.75 day have been filtered out. The forecast starts on August 14 (day 0), 1993.

the case, as demonstrated in LR2. As an example, we compute the sequence of 300-m BC.[5] The input time series, which are truncated at day 21.3, are uniformly sampled at $2^8 = 256$ time steps (compared to 1024 steps in LR2). The resulting BC sequence is contoured in Fig. 13. Obviously, there is a clear solitary positive regime around the center during the intrusion event, while in other subregions it is virtually zero; in comparison BT is one order smaller (figure not shown). According to the identification criteria, a baroclinic instability is taking place here.

If one observes more closely, the baroclinic instability has a distinct spatial-temporal structure. The hotspot does not stand still. It originally resides near the western boundary, then moves into the interior, where it halts and amplifies, and diminishes to zero by day 9 (August 23), just after the front intrudes. That is to say, the instability originally appears in the west. Disturbances are introduced eastward into the domain along the front, in a form of spatial growing mode. After day 5 (August 19), the disturbances become strong enough to counteract the propagation. Correspondingly the process is switched into a time growing mode, leading to the meandering intrusion.

The above BC evolution pattern and its clear physics connection demonstrate that, when scale window bounds can be identified, our localized instability theory makes dealing with certain class of dynamical inference problems, particularly highly nonlinear problems, straightforward. Even regardless of nonlinearity, one may notice that it is not easy for the previous linear localized Eulerian instability theory to apply here because of the irregular background field. For example, the large-scale temperature series in Fig. 12a (dashed line) is not a straight line, nor a sinusoidal curve. Our framework admits arbitrary background shape, and hence works for generic purposes.

[5] The depth and time steps are chosen the same as that in Fig. 9 of LR2. The result is similar to but slightly different from the latter, as we are using the updated codes of MS-EVA which has been optimized since the publication of LR2.
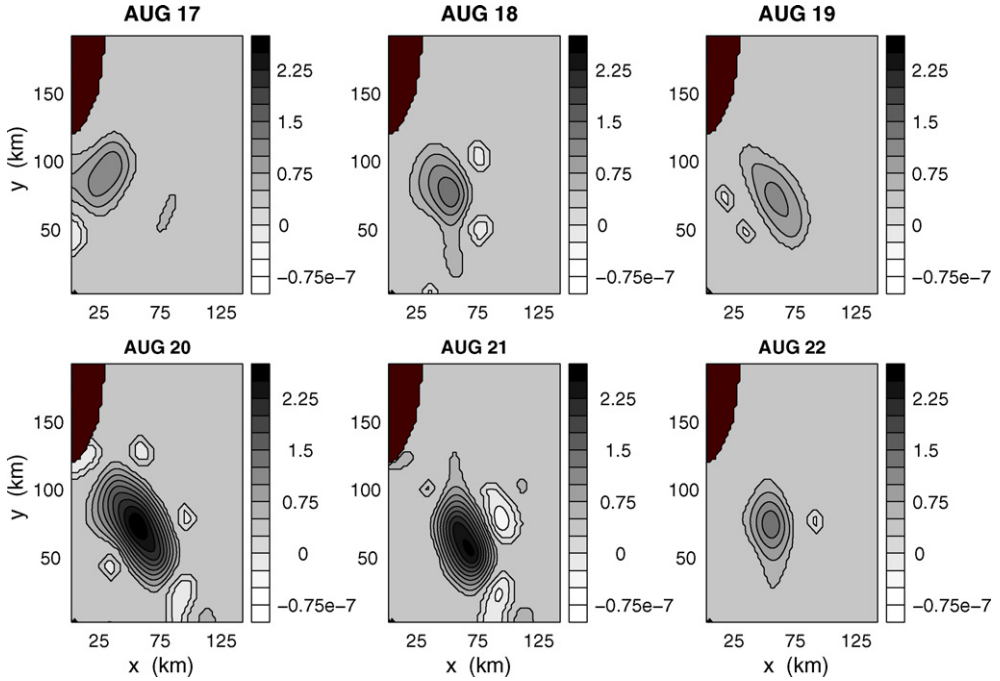
Fig. 13. BC evolution for the IFF region from August 17 through 22, 1993 at depth 300 m. The units are in m^2/s^3.

8. Summary and conclusions

We have developed a localized instability analysis to investigate real oceanic and atmospheric processes which are in nature finite in amplitude and intermittent in space and time. Criteria have been established and validated for the identification of barotropic and baroclinic instabilities from rather generic and complex GFD flows. In the validation, a frontal meandering intrusion has been diagnosed as a highly localized nonlinear Eady-like baroclinic instability which appears as a spatially growing mode then locks into a temporally growing mode. We also found that a local perturbation burst does not necessarily imply a local instability (the perturbation energy could be advected from other processes occurring elsewhere), and that our concept of perfect transfer gives a faithful representation of the physics underlying mean–eddy interactions.

In terms of MS-EVA, characterizing the stability of a system are two Eulerian variables, $BC = (T^{0\to1}_{A^1_n,\partial_h\rho} + T^{0\to1}_{A^1_n,\partial_z\rho}) + TA^{0\to1}_{A^1_n}$, and $BT = (T^{0\to1}_{K^1_n,h} + T^{0\to1}_{K^1_n,z})$, which have a field structure, and are thence representative of highly localized processes. Given a flow, it is locally unstable when the local average of $BC + BT$ is positive, and vice versa. The type of instability is further distinguished by the signs of BC and BT: A positive locally averaged BC corresponds to a baroclinic instability, while a positive locally averaged BT implies a barotropic instability. Because of the Eulerian structure and hence the flexibility, the localized instability analysis is particularly of use for open flow problems.

To validate the analysis, we have examined an Eady model, a Kuo model, which admits only baroclinic instability and barotropic instability, respectively, and a real oceanic front problem (IFF). For the Eady model, BT averages to zero, while BC yields a positive residue, just as expected. In more detail, for all vertical levels, BC horizontally averages to a positive quantity.

The potential energy is continuously transferred from the large-scale reservoir to the eddy window, with a uniform distribution in the vertical direction. At the same moment, a significant part of the transfer is converted into the eddy kinetic energy. This conversion occurs mainly at mid-depth, where the converted energy is carried away toward the surface and bottom via vertical pressure work. The final result of the instability is an intensification of both the density perturbation and the velocity perturbation toward the two vertical boundaries, in agreement with the known results.

The IFF meandering intrusion is related to the Eady instability, but it is finite in amplitude (nonlinear) and highly localized in nature. Our analysis yields an almost solitary positive BC center (BT negligible), which clearly implies a baroclinic instability around the intrusion region. The flow is characterized by a spatially growing mode, which is then locked into a temporally growing mode. The energy transfer is from an irregularly evolving background, into an eddy window highly localized within an interval of 2.6 days. The whole process is analyzed easily with our formalism which would otherwise be difficult to deal with.

For Kuo's cosine jet model, BT averages to a positive quantity, indicating a barotropic instability process. This instability has a meridionally structure, which is not identifiable in the classical framework. The most conspicuous feature is that there exist two narrow strips at the two flanks where the energy transfer is negative. That is to say, the system is locally stable, even though the eddy energy is growing. The moral of this study is that *perturbation growth does not necessarily correspond to instability*, and that underlying the mean–eddy structure interaction there is a mechanism which has been faithfully represented by our perfect transfer (in this case, BT). This striking negative transfer embedded in an unstable field provides a touchstone for our localized instability theory.

The inverse transfer allows for a circulation of energy within the energetic scenario in a Kuo-type barotropic instability. The large-scale KE is first transferred toward the eddy window, within two critical latitudes resembling two "walls" of an "energetic well" around the jet core. The transferred energy is redistributed by $\Delta_y Q_{K_n^1}$, which directs it poleward, but the redistribution stops near the walls, barely going further. The energy thus accumulated near the two critical latitudes has been observed to transfer back toward the large-scale window, acting as an inverse cascade to the background system.

We close this paper by remarking that the marginalization–localization strategy used in this study to localize instabilities may have interesting scientific and practical implications. Certain dynamics inference problems might be tackled in a similar way. Information lost in a classical framework could be retrieved with the aid of some localized mathematical machinery, and quantities global in nature made field-like. In doing so, many GFD theories developed on a global basis could be reconciled to realistic oceanic and atmospheric problems.

Acknowledgments

Appendix A. Generation of the Eady datasets

Originally, Eady (1949) built his model from a frictionless primitive equation set on an f-plane with Bousinesq and hydrostatic approximations. The model domain extends infinitely in either horizontal direction, and is bounded at $z = 0$ and $z = -H$ by two rigid-lids. It has a basic velocity $(\bar{u}, 0, 0)$ and a mean density profile $\bar{\rho}$ such that $(\partial \bar{u}/\partial z) = \Lambda = \text{const}$, $\bar{\rho} = B_y y + B_z z$. Assume an exponential dependence $e^{i(kx+ly-\omega t)}$ for the perturbation fields, where the frequency $\omega = \omega_r + i\omega_i$ is complex, and write $\xi = (\bar{u}k - \omega)/f$, $\sigma = (l/k)$, $R_i = -(gB_z/\rho_0\Gamma^2)$, $R_\sigma = (1 + \sigma^2)R_i$, $\alpha = -(\sqrt{R_\sigma}/2f)\Lambda Hk$. Eady shows that, when $R_i \gg 1$ and $|\xi^2| \ll 1$, the problem has a nontrivial solution if and only if

$$
\begin{cases}
\omega_r = \dfrac{k}{2}(\bar{u}(0) + \bar{u}(-H)) \\[2mm]
\omega_i = \gamma \dfrac{f}{\sqrt{R_\sigma}}, \quad \gamma^2 = (\alpha - \tanh\alpha)(\coth\alpha - \alpha).
\end{cases}
\tag{A.1}
$$

Unstable solutions exist only if $|\alpha| < \alpha_{\text{crt}} \approx 1.1997$. Correspondingly the eigenfunctions are:

$$
\tilde{w}(z) = \left(\frac{1-\xi}{1+\xi}\right)^{i\frac{\sigma}{2}} \cdot C_1 e^{\sqrt{R_\sigma}\xi}(1 - \sqrt{R_\sigma}\xi) + C_2 2^{-\sqrt{R_\sigma}\xi}(1 + \sqrt{R_\sigma}\xi),
\tag{A.2}
$$

$$
\tilde{u}(z) = -\frac{\Lambda/f}{1+\sigma^2}\left[-\frac{\sigma}{\xi}\frac{d\tilde{w}}{d\xi} - i\left(\sigma^2\frac{\tilde{w}}{\xi} + \frac{d\tilde{w}}{d\xi}\right)\right],
\tag{A.3}
$$

$$
\tilde{v}(z) = -\frac{\Lambda/f}{1+\sigma^2}\left[\frac{1}{\xi}\frac{d\tilde{w}}{d\xi} + i\sigma\left(\frac{\tilde{w}}{\xi} - \frac{d\tilde{w}}{d\xi}\right)\right],
\tag{A.4}
$$

$$
\tilde{P}(z) = -\frac{\Lambda/f}{1+\sigma^2} \cdot \frac{f\rho_0}{ik} \cdot \left[\left(\frac{1}{\xi}\frac{d\tilde{w}}{d\xi} + i\sigma\frac{\tilde{w}}{\xi}\right) + \left(\tilde{w} - \xi\frac{d\tilde{w}}{d\xi}\right)\right],
\tag{A.5}
$$

$$
\tilde{\rho}(z) = \frac{\Lambda/f}{1+\sigma^2} \cdot \frac{fa\rho_0}{g} \cdot \frac{i}{\xi} \cdot \left[\left(\frac{1}{\xi}\frac{d\tilde{w}}{d\xi} + R_\sigma\tilde{w}\right) + i\sigma\left(\frac{\tilde{w}}{\xi} - \frac{d\tilde{w}}{d\xi}\right)\right],
\tag{A.6}
$$

where the constants C_1 and C_2 are related through

$$
\frac{C_2}{C_1} = -e^{-2\sqrt{R_\sigma}\xi(0)}\left(\frac{1 - \sqrt{R_\sigma}\xi(0)}{1 + \sqrt{R_\sigma}\xi(0)}\right).
$$

In these equations, all variables are dimensional.

We choose the following configuration to generate the Eady datasets:

$\rho_0 = 1025$ kg/m^3	$H = 1000$ m
$\bar{u}_0 = 20$ cm/s	$\bar{u}_{-H} = 10$ cm/s
$B_z = -1 \times 10^{-2}$ kg/m^4	$f = 1 \times 10^{-4}$ Hz

It is easy to check that the two conditions under which the Eady solution is valid are satisfied. Without losing generality, let $l = 0$. The shortwave cut-off (corresponding to α_{crt}) associated with

(A.2)–(A.6) is then $k_{crt} = 2.454 \times 10^{-5}\,\text{m}^{-1}$. Given a $k < k_{crt}$, an unstable solution is obtained, and correspondingly a dataset can be generated. We now check its consistency.

For a dataset to be consistent for the MS-EVA application, its time sequences should be: (1) long enough to span some integer cycle(s), otherwise aliasing effects will come in and give a spurious basic flow for the decomposition; (2) short enough that the amplitude of perturbation is within the tolerance of a valid linear solution. These requirements can be satisfactorily met if we choose an unstable system with perturbation large in frequency while small in growth rate, i.e., $|\omega_r| \gg |\omega_i|$. By (A.1), if we have k distinctly larger than zero, and at the same time let $\gamma \to 0$, then this condition is satisfied. Such k's lie near the critical wavenumber k_{crt} (notice $k \propto \alpha$ when $l = 0$). We choose $k = 1 \times 10^{-5}\,\text{m}^{-1}$, which gives an $\omega = 1.50 \times 10^{-6} + 2.53 \times 10^{-7}\text{i}\,\text{rad/s}$, meeting the above requirements.

With the eigenvalue and eigenvector, we compute the solutions of all the fields and truncate them at exactly the end of the second cycle to form a series for each data point. The series length is thence

$$2 \times \frac{2\pi}{\omega_r} \approx 8.38 \times 10^6\,\text{s} = 97\,\text{days}.$$

Within this interval, disturbances grow at most by $\exp(8.38 \times 10^6 \omega_i) \approx 8.31$ times. So, if initially the perturbation is set smaller than the basic field by $(1/8.31)\varepsilon$ (ε the permissible relative magnitude for a linear disturbance), then the solution will be valid throughout the 97-day time duration. This can be done by properly manipulating the constant C_1 of $W(z)$ in (A.2). Let $C_1 = 2 \times 10^{-7}$. It yields a maximal $|u'|/\bar{u} < 10^{-3}$, which is much smaller than the Rossby number $Ro = (U/fL) \sim 10^{-2}$.

Apart from the unstable solution, we also need to examine the energetics for a stable mode and a neutrally stable mode. We choose for the two modes $k = 3 \times 10^{-5}\,\text{m}^{-1} > k_{crt}$ and $k = k_{crt} = 2.454 \times 10^{-5}\,\text{m}^{-1}$, which yield $\omega_r = 4.04 \times 10^{-6}\,\text{rad/s}$ and $\omega_r = 3.68 \times 10^{-6}\,\text{rad/s}$, respectively. Again, the solution series are truncated at the end point of the second cycle (36 days and 39 days in length, respectively). The three chosen solutions are sampled at $2^{10} = 1024$ time instants, and mapped onto an Arakawa B-grid with a mesh of 20 km $\times$ 50 km $\times$ 100 m (50 points in x, 20 points in y, and 10 levels in z). The datasets obtained are now ready for the MS-EVA application.

Appendix B. Kuo's barotropic instability model

We consider a primitive equation version of Kuo's model (Kuo, 1949, 1973). On an f-plane, equations governing the 2D perturbations from a zonal barotropic jet $\bar{u} = \bar{u}(y)$ are reduced to

$$\frac{d^2\tilde{v}}{dy^2} + \left(\frac{\bar{u}_{yy}}{c - \bar{u}} - k^2 \right) \tilde{v} = 0, \tag{B.1}$$

where $\tilde{v}$ is the amplitude of perturbation y-velocity, $c = \omega/k$ the phase speed, and $\bar{u}_{yy} = (d^2\bar{u}/dy^2)$ the gradient of the background potential vorticity. In a channel bounded to the north and south, respectively by $y = L$ and $y = -L$, the boundary condition is

$$\tilde{v} = 0, \quad \text{at } y = \pm L. \tag{B.2}$$

Eqs. (B.1) and (B.2) form the eigenvalue problem of barotropic instability.

Consider a cosine background jet [see Eq. (23)]. The above eigenvalue problem is solved with the approach by Kuo (1949) (see also, Kuo, 1973; Pedlosky, 1979). We need a neutrally stable solution and an unstable solution. For the former, there exists an eigenvalue (phase speed) $c = \bar{u}(y_c) = (1/2)\bar{u}_{\max}$ which gives a wavenumber $k = (\sqrt{3}/2)\pi/L$, and an eigen-amplitude for the meridional velocity $\tilde{v} = \bar{u}_{\max} \cos(\pi y/2)$.

The choosing of the unstable mode is not arbitrary. For a valid dataset, the eigenvalue $c = c_r + \mathrm{i}c_i$ must be such that $|c_i| \ll |c_r|$ while c_i is significantly greater than zero. As in the Eady case, a k near its critical value $(\sqrt{3}/2)(\pi/L)$ (on the unstable side, of course) will yield such a solution. We choose $k = 0.75(\pi/L)$. Use the shooting method (e.g., Press et al., 1992) to solve (B.1). The convergence is usually very fast, and the resulting eigenvalue thus obtained is $c = c_r + \mathrm{i}c_i = (0.4504 + 0.0476\mathrm{i})\bar{u}_{\max}$. Clearly $|c_i|$ is much smaller than $|c_r|$, allowing an extraction of several cycles from the solution to form the dataset. In obtaining the eigenfunction, the magnitude of $|\tilde{v}_r|$ has been made small so as to have the solution valid throughout.

To generate the datasets, choose $L = 100$ km, $\bar{u}_{\max} = 1$ m/s, $f = 10^{-4}$ 1/s, which are typical of western ocean jets, and let x run over $[-2L, 2L]$, and t span exactly two cycles (approximately 21 days for the neutrally stable mode and 14 days for the unstable mode). With the k's chosen, the x extends at least one wavelength for either of the datasets, allowing an application of the zonal average whenever necessary. The solutions are mapped on an Arakawa B-grid with 40×80 grid points ($\Delta x = 10$ km, $\Delta y = 0.5$ km), and sampled at $2^{10} = 1024$ time moments. These gridded solution sequences are now ready for MS-EVA.

References

Cushman-Roisin, B., 1994. Introduction to Geophysical Fluid Dynamics. Prentice Hall, 320 pp.

Eady, E.T., 1949. Long waves and cyclone waves. Tellus 1, 258–277.

Harrison, D.E., Robinson, A.R., 1978. Energy analysis of open regions of turbulent flows-mean eddy energetics of a numerical ocean circulation experiment. Dyn. Atmos. Oceans 2, 185–211.

Holton, J.R., 1992. An Introduction to Dynamic Meteorology. Academic Press, 496 pp.

Kuo, H.L., 1949. Dynamic instability of two-dimensional non-divergent flow in a barotropic atmosphere. J. Meteorol. 6, 105–122.

Kuo, H.L., 1973. Dynamics of quasigeostrophic flows and instability theory. In: Yih, C.-S. (Ed.), In: Advances in Applied Mechanics, vol. 13. Academic Press, pp. 247–330.

Liang, X.S., 2002. Multiscale window transform and multiscale energy and vorticity analysis. Harvard Reports in Physical/Interdisciplinary Ocean Science, Rep. No. 66, Harvard University, Cambridge, MA, 411 pp.

Liang, X.S., Anderson, D.G.M., 2007. Multiscale window transform. SIAM J. Multiscale Model. Simul. 6 (2), 437–467.

Liang, X.S., Robinson, A.R., 2005. Localized multiscale energy and vorticity analysis. I. Fundamentals. Dyn. Atmos. Oceans 38, 195–230.

Liang, X.S., Robinson, A.R., 2004. A study of the Iceland–Faeroe Frontal variability with the multiscale energy and vorticity analysis. J. Phys. Oceanogr. 34, 2571–2591.

Liu, Y., Mu, M., 1996. Nonlinear stability theorem for Eady's model of quasigeostrophic baroclinic flow. J. Atmos. Sci. 53 (10), 1459–1463.

Miller, A.J., et al., 1995. Quasigeostrophic forecasting and physical processes of Iceland–Faeroe Frontal variability. J. Phys. Oceanogr. 25, 1273–1295.

Mu, M., Shepherd, T.G., 1994. Nonlinear stability of Eady's model. J. Atmos. Sci. 51, 3427–3436.

Pedlosky, J., 1979. Geophysical Fluid Dynamics. Springer-Verlag, 624 pp.

Pierrehumbert, R.T., Swanson, K.L., 1995. Baroclinic instability. Ann. Rev. Fluid Mech. 27, 419–467.

Pinardi, N., Robinson, A.R., 1986. Quasigeostrophic energetics of open ocean regions. Dyn. Atmos. Oceans 10, 185–219.

Press, W.H., Teukolsky, S.A., Vertterling, W.T., Flannery, B.P., 1992. Numerical Recipes in C—The Art of Scientific Computing, 2nd ed. Cambridge University Press, 965 pp.

Robinson, A.R., Arango, H.G., Miller, A.J., Warn-Varnas, A., Poulain, P.-M., Leslie, W.G., 1996. Real-time operational forecasting on shipboard of the Iceland–Faeroe Frontal variability. Bull. Am. Meteorol. Soc., 243–259.
Tennekes, H., Lumley, J.L., 1972. A First Course in Turbulence. MIT Press.
Wiggins, S., 2003. Introduction to Applied Nonlinear Dynamical Systems and Chaos, 2nd ed. Springer.